Journal of Computational Physics 344 (2017) 303–319

Contents lists available at ScienceDirect

Journal of Computational Physics

www.elsevier.com/locate/jcp

A robust bi-orthogonal/dynamically-orthogonal method using the covariance pseudo-inverse with application to stochastic flow problems

Hessam Babaee [a,*], Minseok Choi [b], Themistoklis P. Sapsis [a], George Em Karniadakis [b]

[a] Massachusetts Institute of Technology, Cambridge, MA 02139, USA
[b] Division of Applied Mathematics, Brown University, Providence, RI 02912, USA

ARTICLE INFO

Article history:
Received 4 May 2016
Received in revised form 18 April 2017
Accepted 21 April 2017
Available online 5 May 2017

Keywords:
Stochastic Navier–Stokes equations
Uncertainty quantification
Reduced order modeling
Dynamical orthogonality
Bi-orthogonality

ABSTRACT

We develop a new robust methodology for the stochastic Navier–Stokes equations based on the dynamically-orthogonal (DO) and bi-orthogonal (BO) methods [1–3]. Both approaches are variants of a generalized Karhunen–Loève (KL) expansion in which both the stochastic coefficients and the spatial basis evolve according to system dynamics, hence, capturing the low-dimensional structure of the solution. The DO and BO formulations are mathematically equivalent [3], but they exhibit computationally complimentary properties. Specifically, the BO formulation may fail due to crossing of the eigenvalues of the covariance matrix, while both BO and DO become unstable when there is a high condition number of the covariance matrix or zero eigenvalues. To this end, we combine the two methods into a robust hybrid framework and in addition we employ a pseudo-inverse technique to invert the covariance matrix. The robustness of the proposed method stems from addressing the following issues in the DO/BO formulation: (i) eigenvalue crossing: we resolve the issue of eigenvalue crossing in the BO formulation by switching to the DO near eigenvalue crossing using the equivalence theorem and switching back to BO when the distance between eigenvalues is larger than a threshold value; (ii) ill-conditioned covariance matrix: we utilize a pseudo-inverse strategy to invert the covariance matrix; (iii) adaptivity: we utilize an adaptive strategy to add/remove modes to resolve the covariance matrix up to a threshold value. In particular, we introduce a soft-threshold criterion to allow the system to adapt to the newly added/removed mode and therefore avoid repetitive and unnecessary mode addition/removal. When the total variance approaches zero, we show that the DO/BO formulation becomes equivalent to the evolution equation of the Optimally Time-Dependent modes [4]. We demonstrate the capability of the proposed methodology with several numerical examples, namely (i) stochastic Burgers equation: we analyze the performance of the method in the presence of eigenvalue crossing and zero eigenvalues; (ii) stochastic Kovasznay flow: we examine the method in the presence of a singular covariance matrix; and (iii) we examine the adaptivity of the method for an incompressible flow over a cylinder where for large stochastic forcing thirteen DO/BO modes are active.

* Corresponding author.
E-mail address: hbabaee@pitt.edu (H. Babaee).

http://dx.doi.org/10.1016/j.jcp.2017.04.057
0021-9991/

1. Introduction

Recently, there has been a growing interest in quantifying parametric uncertainty in physical and engineering problems through the probabilistic framework. Such problems are often described by Stochastic Partial Differential Equations (SPDEs), and they arise in various fields such as fluid mechanics, solid mechanics, wave propagation through random media [5–7], random vibrations [8–10], finance [11], etc. The source of stochasticity in all the above cases includes uncertainty in physical parameters, initial and/or boundary conditions, random excitations, etc. All these stochastic elements may be modeled as random processes or random variables. Several methods have been developed to study SPDEs, including Monte Carlo (MC) method and its variants such as multi-level MC and Quasi-MC (QMC) [11–13] and, more recently, generalized Polynomial Chaos (gPC), Multi-Element generalized Polynomial Chaos (MEgPC), Probabilistic Collocation Method (PCM), Multi-Element Probabilistic Collocation Method (MEPCM) and many other variants (see e.g. [14–27] and references therein).

Another approach to uncertainty quantification is order-reduction schemes or Reduced-Order Models (ROMs) for the simplification and analysis of high-dimensional complex systems. Many methods in ROMs have been developed in the context of deterministic framework such as Proper Orthogonal Decomposition (POD) or Principal Component Analysis (PCA) with applications to many disciplines such as turbulent fluid flows [28,29], structural vibrations [30,31], image processing [32], signal processing and data compression to name a few. However, there have been a few research studies on ROMs in the context of stochastic framework. To this end, the Karhunen–Loéve decomposition turns out to be useful as it provides a low-dimensional representation for second-order random fields as it is optimal in the mean square sense.

A new methodology was developed in [1,33] in which a generalized KL expansion of the form

$$u(x,t;\omega) = \bar{u}(x,t) + \sum_{i=1}^{N} \sqrt{\lambda_i}\phi_i(x,t)\eta_i(t;\omega), \quad \omega \in \Omega \tag{1}$$

is considered, where N is the number of modes, $\bar{u}(x,t)$ is the mean, λ_i and $\phi_i(x,t)$ are the eigenvalues and eigenfunctions of the spatial basis, respectively, and $\eta_i(t;\omega)$ are zero-mean stochastic processes. In [1], exact evolution equations for the mean, spatial basis and the stochastic coefficients are derived. In the above representation both the spatial basis $\phi_i(x,t)$ and the stochastic basis $\eta_i(t;\omega)$ evolve in time unlike other methods such as gPC or POD. The time redundancy in both the spatial basis and the stochastic coefficients is removed by imposing the so called *Dynamical Orthogonality (DO) condition*. The DO method has been applied in several application including fluid flows [34,35]. A theoretical bound for the approximation error of the DO solution was obtained for the case of a linear parabolic equation with random data in [36].

Recently, Cheng et al. [2] adopted the same time-dependent representation used in [1]. By imposing static constraints on both the spatial and the stochastic basis, the so called *Bi-Orthogonal (BO) condition*, an independent set of equations describing the evolution of all the quantities involved (BO evolution equations) was obtained. Although in both studies the same projections were employed (with respect to physical and stochastic space) the equations rely on different conditions imposed on the same representation. Similar ideas have been proposed earlier to this work in quite different fields, namely chemistry and quantum mechanics for the approximation of the deterministic Schrodinger equations by the Multi Configuration Time Dependent Hartree (MCTDH) method [37,38], and later by Koch and Lubich [39].

In the approximation given by equation (1), the solution may need a different number of terms to represent the solution within a prescribed accuracy e.g. due to the nonlinearity of the system. In such cases, we need to adaptively add or remove modes to better capture the transient behavior. In [40] a set of energy-based adaptive criteria was developed for the evolution of the stochastic subspace dimensionality. The newly added modes must have small energy at some threshold value above which the covariance energy is resolved. Similarly, the mode removal occurs for modes with low energy. The existence of low energy modes, i.e. small eigenvalues of the covariance matrix, in both BO and DO equations renders these systems highly ill-conditioned, and for zero eigenvalue they become unstable. As it was observed in [41] for deterministic initial conditions, the covariance matrix in the DO formulation is singular and the authors suggest using a Pseudo-Inverse (PI) technique to invert the covariance matrix. Similarly, the issue of rank overestimation leads to ill-conditioned matrices in dynamical low-rank approximations. To overcome the numerical instability arising from inverting the ill-conditioned matrices, in [42], a splitting scheme for matrix and linear differential operators was proposed. As we will demonstrate in this study, the BO formulation also suffers from an ill-conditioned covariance matrix or zero eigenvalue.

The precise mathematical relationship between the two methods was established rigorously in [3]; the methods are equivalent in the sense that one can be derived from the other through an invertible and linear transformation governed by an orthogonal matrix differential equation. Moreover, BO becomes unstable when there is an eigenvalue crossing, while it preserves a diagonal covariance matrix for all times. It was shown in [3] that absent of eigenvalue crossing, numerically BO performs better than DO. It is, therefore, advantageous to use BO as the dominant solver and switch to DO only when eigenvalue crossings are detected. To this end, we propose a unified hybrid framework of the two methods for SPDEs as a reduced-order modeling approach: (1) by utilizing an invertible and linear transformation between them where we switch from BO to DO when facing an eigenvalue crossing, and (2) by employing a pseudo-inverse technique for inverting the covariance matrix. We will refer to this hybrid approach as the robust PI BO/DO method.

The structure of the paper is as follows. In Section 2 we briefly review DO and BO representations, their corresponding evolution equations and the equivalence between BO and DO along with the matrix differential equation. In Section 3 we propose a pseudo-inverse strategy for dealing with singular and near singular covariance matrix along with a soft-threshold

criterion for adaptive mode addition/removal. In Section 4 we present three problems to illustrate the proposed methodology: (i) one-dimensional stochastic Burgers equation; (ii) stochastic Kovasznay flow, and (iii) stochastic incompressible flow over cylinder. We conclude the paper with a brief summary in Section 5.

2. Mathematical formulation

In this section we briefly review BO and DO formulations [1,43,3,2].

2.1. Definitions

Let $(\Omega, \mathcal{F}, P)$ be a probability space, where Ω is the sample space, $\mathcal{F}$ is the σ-algebra of subsets of Ω, and P is a probability measure. For a random field $u(x,t;\omega)$, $\omega \in \Omega$, the expectation operator of u is defined as

$$\bar{u}(x,t) \equiv E[u(x,t;\omega)] = \int_{\Omega} u(x,t;\omega) dP(\omega).$$

The set of all continuous and square integrable random fields, *i.e.*, $\int_D E[u(x,t;\omega)^T u(x,t;\omega)]dx < \infty$, where $u(x,t;\omega)^T$ is the transpose of u, for all $t \in T$ and the bi-linear form of the covariance operator

$$C_{u(\cdot,t;\omega)v(\cdot,s;\omega)}(x,y) = E[(u(x,t;\omega) - \bar{u}(x,t))^T (v(x,s;\omega) - \bar{v}(x,s))], \quad x, y \in D,$$

form a Hilbert space that will be denoted by $\mathcal{H}$ [5,44]. For $u(x,t;\omega), v(x,t;\omega) \in \mathcal{H}$, the spatial inner product is defined as

$$< u(\cdot,t;\omega), v(\cdot,t;\omega) >= \int_D u(x,t;\omega)^T v(x,t;\omega) dx.$$

We define the projection operator Φ_S of a random field $u(x,t;\omega), x \in D$ to an m-dimensional linear subspace S spanned by the orthonormal basis $S = \{w_i(x,t;\omega)\}_{i=1}^m, x \in D$ as follows:

$$\Phi_S[u(x,t;\omega)] = \sum_{i=1}^{m} < w_i(\cdot,t;\omega), u(\cdot,t;\omega) > w_i(x,t;\omega)$$

Next, we consider the covariance operator when it acts on an element $u(x,t;\omega), \omega \in \Omega$ for $s = t$:

$$C_{u(\cdot,t;\omega)v(\cdot,t;\omega)}(x,y) = E[(u(x,t;\omega) - \bar{u}(x,t))^T (v(x,t;\omega) - \bar{v}(x,t))], \quad x, y \in D,$$

and the integral operator, based on the covariance operator C at time t, defined by

$$K_C \phi = \int_D C_{u(\cdot,t)u(\cdot,t)}(x,y)\phi(x,t)dx, \quad \phi \in L^2 \tag{2}$$

is a compact, self-adjoint, and positive operator in the Hilbert space of continuous and square integrable fields L^2 equipped with inner product $< \cdot, \cdot >$. Then the KL expansion [45] implies that every random field $u(x,t;\omega) \in \mathcal{H}$ at a given time t can be written in the form given by equation (1), where the eigenvalues and the eigenfunctions are obtained from the following eigenvalue problem:

$$\int_D C_{u(\cdot,t)u(\cdot,t)}(x,y)\phi_i(x,t)dx = \lambda_i \phi_i(y,t), \quad y \in D, \tag{3}$$

where ϕ_i are orthonormalized so that $< \phi_i, \phi_j >= \delta_{ij}$ and $\eta(t;\omega)$ are zero mean, unit variance, and mutually uncorrelated, *i.e.* $E[\eta_i \eta_j] = \delta_{ij}$. The eigenvalues λ_i are non-negative and can be arranged in a decreasing order. Then, every random field $u(x,t;\omega) \in \mathcal{H}$ can be approximated by a finite series expansion with N terms of the expansion given in equation (1). Indeed, it is known that the KL decomposition is optimal in the mean square sense. In the context of numerical method to SPDEs, constraints are required to derive how the components in the above KL decomposition evolve in time; the components $(\lambda_i, \phi_i, \eta_i)_{i=1}^N$ are time-dependent. In the next subsections we review the two methods which have different assumptions on the constraints.

Table 1
The BO and DO conditions. I_N is the $N \times N$ identity matrix and O_N the $N \times N$ zero matrix.

BO	DO
$\langle \mathbf{U}^T\mathbf{U}\rangle = \Lambda, \quad E[\mathbf{Y}^T\mathbf{Y}] = I_N$	$\left\langle \frac{\partial \mathbf{U}^T}{\partial t}\mathbf{U}\right\rangle = O_N$

2.2. Model problem

We consider the following stochastic partial differential equation

$$\frac{\partial u}{\partial t} = F(u(t,x;\omega)), \quad x \in D, \omega \in \Omega, \tag{4a}$$

$$u(t_0,x;\omega) = u_0(x;\omega), \quad x \in D, \omega \in \Omega, \tag{4b}$$

$$\mathcal{B}[u(t,x;\omega)] = h(t,x;\omega), \quad x \in \partial D, \omega \in \Omega, \tag{4c}$$

where F is a differential operator and $\mathcal{B}$ is a linear differential operator, D is a bounded domain in $\mathcal{R}^d$ where $d = 1, 2$, or 3. We assume that the problem is well-posed such that the set of solution $u(x,t;\omega)$ forms a Hilbert space $\mathcal{H} \equiv L_2(D \times \Omega)$ for every t. The randomness may come from different sources including parameters, initial conditions, and boundary conditions.

2.3. The BO and DO evolution equations

In both the BO and DO decompositions the following representation of the solution is considered:

$$u(x,t;\omega) = \bar{u}(x,t) + \sum_{i=1}^{N} u_i(x,t)Y_i(t;\omega) = \bar{u}(x,t) + \mathbf{U}(x,t)\mathbf{Y}^T(t;\omega), \tag{5}$$

where $u_i(x,t)$ are the *spatial basis* and $Y_i(t;\omega)$ the *stochastic basis*. We use the vector notation for simplicity: $\mathbf{U}(x,t) = (u_1(x,t), u_2(x,t), ..., u_N(x,t))$ and $\mathbf{Y}(t;\omega) = (Y_1(t;\omega), Y_2(t;\omega), ..., Y_N(t;\omega))$, and ignore the arguments x, t, ω when there is no ambiguity for simplicity. In the DO formulation a *dynamic constraints* is imposed on the spatial basis, i.e., the evolution of the spatial basis $\mathbf{U}(x,t)$ be *normal* to the space V_S spanned by the spatial basis $\mathbf{U}(x,t)$. This condition is referred to as the *dynamically orthogonal condition*. Note that the DO condition implies that the spatial basis preserves orthonormality in time. In contrast, BO imposes *static constraints* on both the spatial and stochastic basis; the spatial basis is orthogonal while the stochastic basis is orthonormal at every time. The dynamically orthogonal condition and the static constraints are shown in Table 1.

Before presenting the evolution equations for BO and DO we define the following matrices and vectors to simplify the notation:

$$\mathbf{h} = \left\langle \tilde{F}[u], \mathbf{U}\right\rangle \tag{6a}$$

$$\mathbf{p} = E[F[u]\mathbf{Y}] \tag{6b}$$

$$\Lambda = diag(\lambda_1, ..., \lambda_N) \tag{6c}$$

$$C = E[\mathbf{Y}^T\mathbf{Y}] \tag{6d}$$

$$G = \left\langle \mathbf{U}^T E[F[u]\mathbf{Y}]\right\rangle \tag{6e}$$

$$M = E\left[\mathbf{Y}^T \frac{d\mathbf{Y}}{dt}\right] \tag{6f}$$

$$S = \left\langle \mathbf{U}^T \frac{\partial \mathbf{U}}{\partial t}\right\rangle. \tag{6g}$$

Note that $\lambda_i, i = 1, ..., N$ are the eigenvalues of the covariance matrix. For the BO formulation the covariance matrix is the inner product of the spatial basis, i.e. $\Lambda = <\mathbf{U}^T\mathbf{U}>$, while for the DO formulation the covariance matrix is $C = E[\mathbf{Y}^T\mathbf{Y}]$.

Remark 1. Deriving closed formulas for M and S is the key to derive the evolution equations for BO and DO as they contain the information of how the spatial and stochastic bases evolve in time. It has been shown in [1–3] that there exist unique and closed formulas for M and S for BO and DO based on the BO and DO condition. For the DO formulation

$$S = O_N, \quad M = G^T, \tag{7}$$

where O_N is the N-by-N zero matrix. For the BO formulation deriving S and M is more involved but utilizing the BO condition yields the following closed formula [3]:

Table 2
The BO and DO evolution equations. $\mathbf{U}^{DO}$ and $\mathbf{Y}^{DO}$ are the DO components of the spatial and stochastic basis, respectively, and $\mathbf{U}^{BO}$ and $\mathbf{Y}^{BO}$ are the BO components.

	DO	BO
Mean	$\frac{\partial \bar{\mathbf{u}}^{DO}}{\partial t} = E[F(u)]$	$\frac{\partial \bar{\mathbf{u}}^{BO}}{\partial t} = E[F(u)]$
Spatial basis	$\frac{\partial \mathbf{U}^{DO}}{\partial t} = (\mathbf{p} - \mathbf{U}^{DO} G)C^{-1}$	$\frac{\partial \mathbf{U}^{BO}}{\partial t} = \mathbf{U}^{BO} M + \mathbf{p}$
Stochastic basis	$\frac{d\mathbf{Y}^{DO}}{dt} = \mathbf{h}$	$\frac{d\mathbf{Y}^{BO}}{dt} = (-\mathbf{Y}^{BO} S^T + \mathbf{h})\Lambda^{-1}$

$$M_{ij} = \begin{cases} \frac{G_{ij}+G_{ji}}{-\lambda_i+\lambda_j}, & \text{if } i \neq j \\ 0, & \text{if } i = j \end{cases} \tag{8a}$$

$$S_{ij} = \begin{cases} G_{ij} + \lambda_i M_{ij}, & \text{if } i \neq j \\ G_{ii}, & \text{if } i = j. \end{cases} \tag{8b}$$

Note that M is skew-symmetric while S is almost skew-symmetric meaning that the diagonal entries are non-zero.

The BO and DO evolution equations are shown in Table 2. They consist of one deterministic PDE for the mean, N deterministic PDEs for the spatial basis, and N stochastic ODEs for the stochastic basis.

2.4. Equivalence of BO and DO

Let $\check{U} = (\check{u}_1, \check{u}_2, ..., \check{u}_N)$, $\hat{U} = (\hat{u}_1, \hat{u}_2, ..., \hat{u}_N)$, $\check{Y} = (\check{Y}_1, \check{Y}_2, ..., \check{Y}_N)$ and $\hat{Y} = (\hat{Y}_1, \hat{Y}_2, ..., \hat{Y}_N)$ be the BO and DO components, respectively. We consider the linear transformation between the DO and BO components:

$$\check{Y} = \hat{Y} P \Lambda^{-\frac{1}{2}}, \tag{9a}$$

$$\check{U} = \hat{U} P \Lambda^{\frac{1}{2}}, \tag{9b}$$

where P satisfies the matrix differential equation

$$\frac{dP}{dt} = P \Lambda^{-\frac{1}{2}} \Sigma \Lambda^{-\frac{1}{2}}, \qquad P(0) = I_N, \tag{10}$$

where I_N is the $N \times N$ identity matrix, and Σ is the skew-symmetric part of the matrix S in equation (6g), i.e. $\Sigma_{ij} = S_{ij}$ for $i \neq j$ and $\Sigma_{ii} = 0$ for $i = 1, ..., N$. This leads to the following theorem:

Theorem 1. *[3] Suppose that $\check{U}$ and $\check{Y}$ satisfy the BO equations. Assume that the eigenvalues $\lambda_i, i = 1, ..., N$ of the covariance operator in equation (3) are discrete at any time. Then the linear transformation (9a)–(9b) defines a new set of stochastic coefficients and basis elements for which (i) $\check{Y}^T \check{U} = \hat{Y}^T \hat{U}$ the total solution remains invariant, and (ii) $\hat{U}$ satisfies the DO condition. Hence, $(\hat{U}, \hat{Y})$ is a solution of the DO equations. The invertibility of the transformation allows for the application of the Theorem in the inverse direction.*

3. Robust adaptive algorithm

The BO formulation, by construction, preserves the orthogonality of both stochastic and spatial bases. The orthogonality results in a diagonal covariance matrix Λ whose inverse can be cheaply computed. However, the BO evolution equations assume that there is no eigenvalue crossing. In practice, when two eigenvalues are close to each other, the numerical instability can occur due to the singularity (see equation (8a)). On the contrary, the DO evolution equations involve the inverse of the covariance matrix C for the stochastic basis. Both methods, however, become unstable for a singular covariance matrix.

We employ Theorem 1 to switch from BO to DO and vice versa in order to exploit the bi-orthogonality structure of BO and switch to DO when the difference between the eigenvalues is smaller than a threshold value. We refer to this approach as *hybrid BO/DO* and we provide more details in Section 3.1. Moreover, the BO/DO expansion, expressed by equation (5), may not have a fixed number of modes to represent the solution within a prescribed accuracy, e.g. due to the nonlinearity of the system, and in such cases we need to adaptively add modes when the smallest eigenvalue is larger than a certain threshold value or remove modes when the smallest eigenvalue is smaller than a certain threshold value. As we will demonstrate in this paper, the hybrid formulation can facilitate this adaptation more readily in a robust manner. Since the mode removal/addition occurs at small threshold energy levels, the issue of near-singular covariance must be dealt with. To address this problem we use the *pseudo-inverse* of the covariance matrix as it will be explained in Section 3.3.

3.1. Hybrid BO/DO algorithm

In order to avoid the issue of eigenvalue crossing in the BO formulation, when at time t_c the difference between two eigenvalues is less than a threshold value ϵ_c, i.e. $|\lambda_i(t_c) - \lambda_j(t_c)| < \epsilon_c$, we switch from the BO to the DO via the transformation given by equations (9a)–(9b), which is obtained from solving the matrix differential equation (10). Once the difference between the two closest eigenvalues surpasses the threshold value, i.e. $|\lambda_i(t_c) - \lambda_j(t_c)| \geq \epsilon_c$, we switch back from DO to BO via the transformation given by equations (9a)–(9b).

3.2. Soft threshold: adding and removing modes

The eigenvalues determine the energy (variance) of the system and they are easily computed; for BO they are the diagonal entries of the covariance matrix of the spatial basis $< \breve{U}^T, \breve{U} >$, while for DO they are the eigenvalues of the covariance matrix of the stochastic basis $E[\hat{Y}^T \hat{Y}]$. The objective of an adaptive strategy is to resolve the energy of the system up to some threshold value denoted by σ_{th}. Let us assume that there are N modes and eigenvalues are sorted in a decreasing order, i.e. $(\lambda_1, \lambda_2, ..., \lambda_N)$ where $\lambda_1 \geq \lambda_2 \geq \cdots \geq \lambda_N$. In principle, the last mode must be removed if its energy λ_N falls below the threshold value, i.e. $\lambda_N < \sigma_{th}$. On the other hand, a mode must be added if the energy of the last mode exceeds the threshold value, i.e. $\lambda_N > \sigma_{th}$. We refer to this condition as *hard-threshold* criterion. However, in cases where the energy of the newly added mode decreases, the hard-threshold criterion may trigger unnecessary repetitive mode addition/removal — an undesirable outcome. We, instead, propose a *soft-threshold* criterion. In this approach, a neighborhood centered around the threshold value σ_{th} is considered. The neighborhood is set in the log scale and it is specified by $|\log\lambda - \log\sigma_{th}| < d$, where $d > 0$ is the radius of the neighborhood in the log scale. Therefore, the upper and lower bounds of the neighborhood are given by $\sigma_{th}^+ = 10^d \sigma_{th}$ and $\sigma_{th}^- = 10^{-d}\sigma_{th}$, respectively. In this strategy a new mode with the energy of σ_{th} is added if the energy of the last mode is above the upper bound of the neighborhood, i.e. $\lambda_N > \sigma_{th}^+$. Correspondingly, the last mode is removed if its energy falls below the lower bound of the neighborhood, i.e. $\lambda_N < \sigma_{th}^-$. The soft-threshold criterion effectively creates a *buffer zone* in which the newly added or removed mode is allowed to adjust to system dynamics. The relaxation of the threshold criterion prevents repetitive mode addition/removal that may occur in the hard-threshold strategy.

The newly added mode to the BO/DO decomposition $\{Y_i(t;\omega), u_i(x,t)\}_{i=1}^N$ is chosen from the orthogonal complement of the space spanned by the N active modes, i.e. $Y_{N+1}(t;\omega) \perp \text{span}\{Y_i(t;\omega)\}_{i=1}^N$ and $u_{N+1}(x,t) \perp \text{span}\{u_i(x,t)\}_{i=1}^N$. Other than choosing the new mode from the orthogonal complement of active BO/DO modes, the direction of the newly added mode is chosen arbitrarily. As stated in reference [46], the optimal state of the new mode is in the direction of fastest growing perturbation in the complement subspace $\{Y_i(t;\omega), u_i(x,t)\}_{i=N+1}^\infty$ when the energy of the new mode approaches zero in the limit. However, since the new mode is usually added with small and finite energy, the direction of the newly added mode is naturally corrected as the new mode evolves.

3.3. Pseudo-inverse: singular covariance matrix

Inherently, the energy threshold σ_{th} has a small magnitude and this will render the covariance matrix near-singular. To resolve this issue, we use a pseudo-inverse technique to compute the inverse of the covariance matrix. In the following, we explain the pseudo-inverse strategy for the DO, however the procedure is identical in the case of the BO formulation. To this end, we compute the singular value decomposition of the covariance matrix:

$$C = U\Sigma U^T, \tag{11}$$

where $\Sigma = \text{diag}(\sigma_1, \sigma_2, \ldots, \sigma_N)$. Since C is a symmetric positive definite matrix, σ_i's are identical to the eigenvalues of C, and U to the eigenvectors, and moreover, $U^T U = I$. Therefore, C^{-1} is:

$$C^{-1} = U\Sigma^{-1}U^T. \tag{12}$$

We denote by $\Sigma' = \text{diag}(\sigma_1', \sigma_2', \ldots, \sigma_N')$ a diagonal matrix whose entries are:

$$\sigma_i' = \max\{\sigma_i, \sigma_{th}\}, \qquad i = 1, 2, \ldots, N. \tag{13}$$

Therefore, the pseudo-inverse of C, denoted by C^+ is obtained by:

$$C^+ = U\Sigma'^{-1}U^T. \tag{14}$$

The above strategy replaces the directions with lower energy than the threshold value with σ_{th} for the purpose of computing the inverse of C. For the BO, the covariance matrix is diagonal and therefore, $\Sigma \equiv \Lambda$, and the above procedure amounts to replacing the diagonal elements of Λ that are smaller than σ_{th} with σ_{th}, when computing Λ^{-1}. We note that the choice of the threshold value for computing the pseudo-inverse could be different from that of the mode addition/removal threshold. The adaptive hybrid approach is shown in Algorithm 1.

Algorithm 1: Switching between the BO and DO.

$t = 0$; is BO = true;
repeat
  if $|\lambda_i - \lambda_j| < \epsilon_c$ *and is BO == true* **then**
    is BO = false; (switch to DO)
  else
    is BO = true;
  end
  if $\sigma_i < \sigma_{th}$ **then**
    $\sigma_i = \sigma_{th}$; (use pseudo inverse)
  end
  if *is BO* **then**
    Integrate BO evolution equations.
  else
    Integrate DO evolution equations.
  end
until $t < t_f$;

4. Numerical examples

In the following subsections, we first study the one-dimensional stochastic Burgers equation to illustrate the hybrid BO-DO method. Then we consider the Kavoasznay with the exact solution. Subsequently, we solve stochastic incompressible flow over cylinder, where we employ the adaptive algorithm to add or remove modes.

4.1. Burgers equation

We consider the following Burgers equation

$$u_t + uu_x = \nu u_{xx} + f(x,t;\omega), \qquad x \in [0, 2\pi], \tag{15}$$

with periodic boundary conditions at the two ends. We use the third-order Adams–Bashforth (AB3) as a time-integrator. For space discretization, we use spectral Fourier method with $Nf = 128$ modes. The stochastic ODE that governs the evolution of $d\mathbf{Y}/dt$, is solved using MEPCM with $Ne = 8$ elements and $q = 32$ quadrature points in each element.

4.1.1. Hybrid BO/DO

We assume that we know the random solution and the stochastic forcing $f(x,t;\omega)$ term is given accordingly. We consider the following solution:

$$u(x,t;\omega) = \bar{u}(x,t) + \sum_{i=1}^{2} y_i(t;\omega)u_i(x,t) \tag{16}$$

where:

$$\bar{u}(x,t) = \sin(x-t),$$
$$y_1(t;\omega) = \sqrt{2\lambda_1(t)}\sin(\pi\xi_1(\omega) - t), \qquad y_2(t;\omega) = \sqrt{2\lambda_2(t)}\cos(\pi\xi_2(\omega) - t),$$
$$u_1(x,t) = \frac{1}{\sqrt{\pi}}\cos(x-t), \qquad u_2(x,t) = \frac{1}{\sqrt{\pi}}\cos(2x-3t),$$

and $\xi_1(\omega)$ and $\xi_2(\omega)$ are independent uniform random variables on $[-1,1]$. Therefore we observe that: $\mathbb{E}[y_i y_j] = \lambda_i \delta_{ij}$, and $< u_i, u_j >= \delta_{ij}, i, j = 1, 2$, where $\lambda_i(t)$ are the eigenvalues of the covariance operator. The corresponding exact mean and DO and BO components for the above solution are given in Table 3. The eigenvalues of the solution are given as follows:

$$\lambda_1(t) = \sin^2(t)$$
$$\lambda_2(t) = \cos^2(3t).$$

We choose $\lambda_1(t)$ and $\lambda_2(t)$ such that they have eigenvalue crossing as well as zero eigenvalues, which makes a suitable benchmark problem to test the algorithm. Fig. 1 shows the eigenvalues of the covariance matrix, where 5 zero eigenvalues and 6 eigenvalue-crossings can be observed. We consider $N = 2$ DO/BO modes that match the number of active modes in the exact solution. For the time advancement, we use the time interval of $\Delta t = \frac{\pi}{1200}$ that will ensure that all of the eigenvalue crossings and zero eigenvalues belong to the set of the discrete times $t_{n+1} = t_n + n\Delta t$, $n = 0, 1, 2, \ldots, N$. This will ensure that the discrete time will hit all the singularities. We will investigate the effect of time interval in this section. For the hybrid DO/BO method, we use $\epsilon_c = 10^{-3}$. The above choice of eigenvalues has a singularity at $t = 0$, since $\lambda_1(0) = 0$.

Table 3
Burgers equation: the exact BO and DO components.

	DO	BO
Mean	$\sin(x-t)$	$\sin(x-t)$
Spatial basis	$u_1(x,t)=\frac{1}{\sqrt{\pi}}\cos(x-t)$ $u_2(x,t)=\frac{1}{\sqrt{\pi}}\cos(2x-3t)$	$u_1(x,t)=\sqrt{\lambda_1(t)}\cos(x-t)$ $u_2(x,t)=\sqrt{\lambda_2(t)}\cos(2x-3t)$
Stochastic basis	$Y_1(t;\omega)=\sqrt{2\lambda_1(t)}\sin(\pi\xi_1-t)$ $Y_2(t;\omega)=\sqrt{2\lambda_2(t)}\cos(\pi\xi_2-t)$	$Y_1(t;\omega)=\sqrt{2}\sin(\pi\xi_1-t)$ $Y_2(t;\omega)=\sqrt{2}\cos(\pi\xi_2-t)$

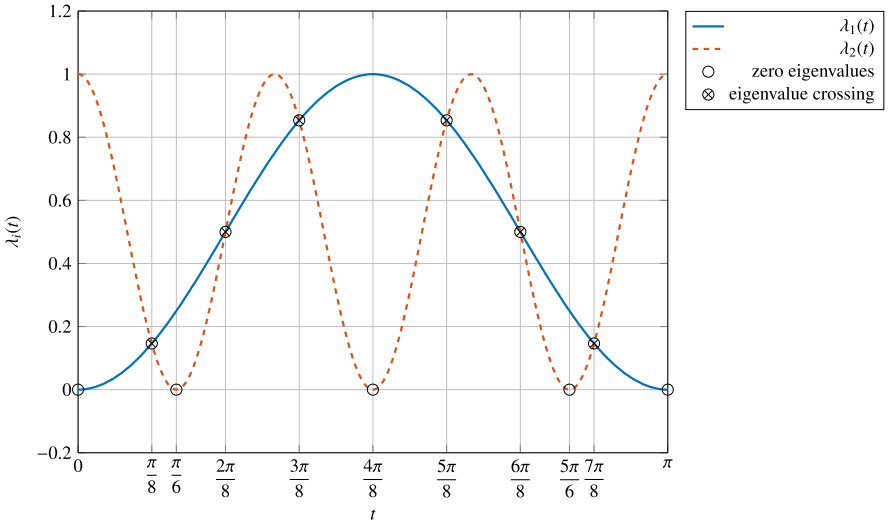

Fig. 1. Exact eigenvalues of the covariance matrix for the stochastic Burgers equation. The eigenvalue crossings and zero eigenvalues are shown by symbols.

To avoid perfect singularity (division by zero) at $t=0$, which leads to NAN values, the evolution of the stochastic system is initialized at $t=10^{-14}$ from the exact solution. This way we preserve the numerical singularity in our stochastic system while avoiding NAN values.

In Fig. 2, the L_2 error curves for the mean and variance of the stochastic Burgers equation for five methods are shown. These methods are: (i) DO, (ii) BO, (iii) DO/BO, (iv) PI DO, and (v) PI DO/BO, where PI implies using the pseudo-inverse technique to compute the covariance matrix. The methods tagged with an upright arrow diverge during their evolution. The eigenvalue crossing does not create numerical instability for DO, and therefore, as it can be seen in Fig. 2, the DO mean and variance errors do not increase at the first eigenvalue crossing at $t=\pi/8$. However, DO diverges at the zero eigenvalue at $t=\pi/6$ where the covariance matrix becomes singular. The BO method diverges at the first eigenvalue crossing at $t=\pi/6$ where matrix M given by equation (8a) becomes singular. To avoid the zero eigenvalue crossing, the hybrid DO/BO method switches from BO to DO before the eigenvalue crossing at $t=\pi/8$, and then it switches back to BO after the eigenvalue crossing. We note that for $0<t<\pi/8$, BO is on in the DO/BO method, and as a result, in this time interval both mean and variance errors of these two methods coincide. The hybrid DO/BO diverges at zero eigenvalue, since at zero eigenvalue the active method is BO and BO is unstable at zero eigenvalue.

Now we use the pseudo-inverse technique to invert the covariance matrix with the threshold of $\sigma_{th}=10^{-7}$. Using the pseudo inverse stabilizes both DO and hybrid DO/BO methods at zero eigenvalues as it can be seen in Fig. 2. We note that the variance errors of PI methods show jumps at zero eigenvalues. This behavior is to be expected in pseudo-inverse methods where the variance of the zero-energy mode is replaced with the finite value of σ_{th}. Among all the methods investigated, PI DO/BO consistently shows smaller values of both mean and variance error than PI DO for all times.

Among the five different methods that we investigated in Fig. 2(a), only the two methods augmented with the pseudo-inverse technique do not diverge, namely: PI DO and PI DO/BO. Now, we investigate the effect of the threshold value σ_{th} for these two methods. In Fig. 3, the L_2 error variations of the mean versus time for four different values of $\sigma_{th}=10^{-3},10^{-5},10^{-7}$, and 10^{-9} are shown. For the threshold value of $\sigma_{th}=10^{-3}$, both methods are stable but show large errors. Similar to the error of BO and DO without using pseudo-inverse, in all cases BO shows less error than DO in the time interval before the first eigenvalue crossing. Note that at $t=0$ the covariance is singular, and the relatively larger error for these two cases is triggered at $t=0$. As a result of this error, the eigenvalues of the DO or BO formulation may not cross and become zero at the discrete times $t_{n+1}=t_n+n\Delta t$, $n=0,1,2,\ldots,N$ and this may result in a stable solution. This behavior is observed for $\sigma_{th}=10^{-3}$ where the error does not increase at the subsequent singularities after $t=0$. As the threshold decreases to $\sigma_{th}=10^{-5}$, the induced error at $t=0$ decreases. The PI DO system shows increase of error after

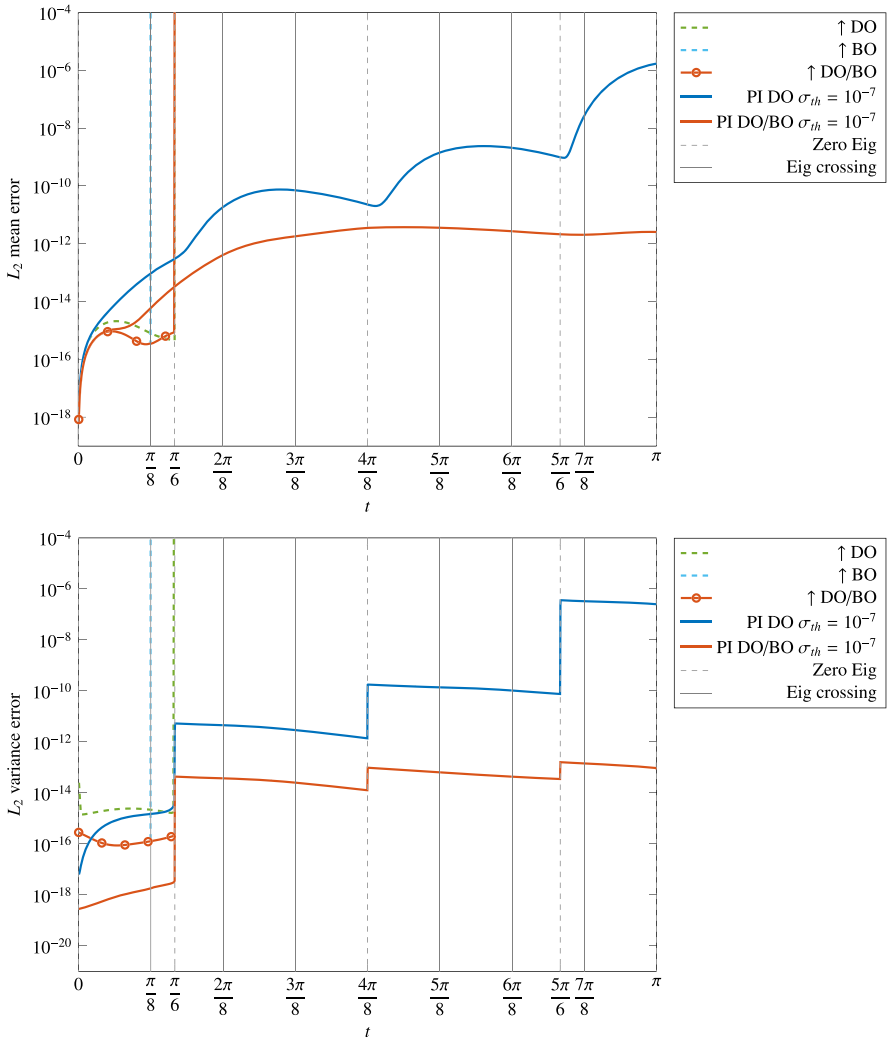

Fig. 2. The L_2 mean (top) and variance (bottom) errors for the stochastic Burgers equation as described in Table 3 for different methods. The upright arrow in the plot legend implies divergence of the method. (For interpretation of the colors in this figure, the reader is referred to the web version of this article.)

each singularity at later times. The PI DO/BO system, on the other hand, shows smaller error compared to the PI DO. For $\sigma_{th} = 10^{-7}$, the PI DO shows significant increase in error after $t = \pi/6$ and it eventually diverges at $t = 4\pi/8$ – the third singularity. The PI DO/BO, however, remains stable and shows the smallest error in all the cases considered in Fig. 3. At the smallest threshold $\sigma_{th} = 10^{-9}$, PI DO diverges at the second singularity at $t = \pi/6$, while the PI DO/BO shows small error until at $t = 5\pi/6$, where a noticeable increase in the error is observed.

The observations made here imply that there exists an optimal threshold value. At large threshold values the energy of the singular or near-singular mode increases excessively by the pseudo-inverse technique, to the point that it itself induces error in the system. For very small values of the threshold the system approaches to the singular behavior, which in turns causes the instability in the numerical algorithm. Clearly, as $\sigma_{th} \to 0$ the original DO or BO systems are retrieved, in which singularity can lead to the blow-up of the solution as it was demonstrated in the discussion of Fig. 2(a). We also observe that the PI DO/BO method consistently shows smaller error, which is indicative of the robustness gained by PI DO/BO method.

As it was explained above the eigenvalues of PI DO and PI DO/BO may not cross or become zero at the discrete times $t_{n+1} = t_n + n\Delta t$, $n = 0, 1, 2, \ldots, N$. To demonstrate the effect of Δt, we compare the results obtained from two different Δt values: (i) $\Delta t = \frac{\pi}{1200}$ which results in an exact matching between the discrete times and the times of all singularities, i.e. eigenvalue crossings and zero eigenvalues, and (ii) $\Delta t' = \frac{\pi+\epsilon}{1200}$ with $\epsilon = 0.01$, that results in discrete times that will not include the times of the singularities.

In Fig. 4, the L_2 error of the mean for DO, BO, DO/BO and PI DO/BO with the two values of $\Delta t = \frac{\pi}{1200}$ and $\Delta t' = \frac{\pi+\epsilon}{1200}$ are shown. The pseudo-inverse threshold value of $\sigma_{th} = 10^{-7}$ is considered for the PI DO/BO formulation. For the case with $\Delta t = \frac{\pi}{1200}$, both DO and DO/BO methods diverge at $t = \pi/6$, and BO diverges at the first eigenvalue crossing at $t = \pi/8$. However, for $\Delta t' = \frac{\pi+\epsilon}{1200}$, small deviation in the time advancement interval averts the numerical instability for DO, BO and

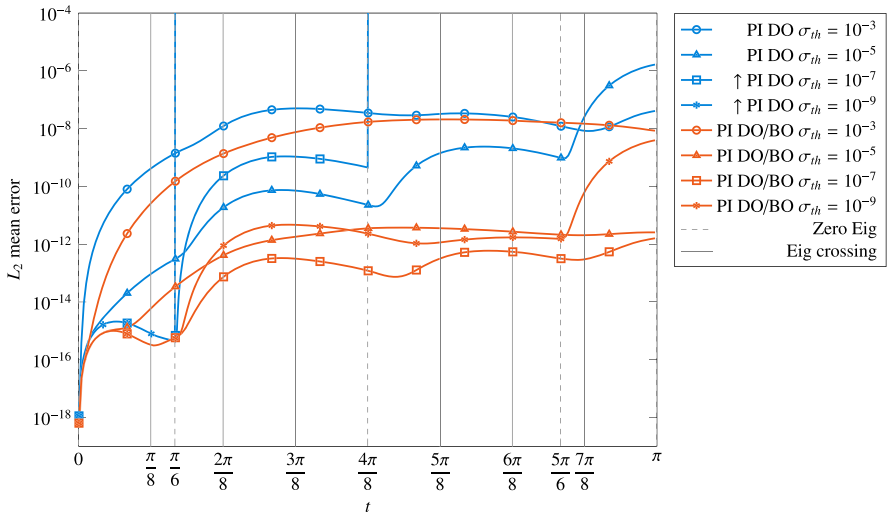

Fig. 3. Stochastic Burgers equation — effect of the threshold value: the L_2 mean error for the stochastic Burgers equation as described in Table 3 for the DO and hybrid DO/BO with pseudo-inverse thresholds σ_{th}. (For interpretation of the colors in this figure, the reader is referred to the web version of this article.)

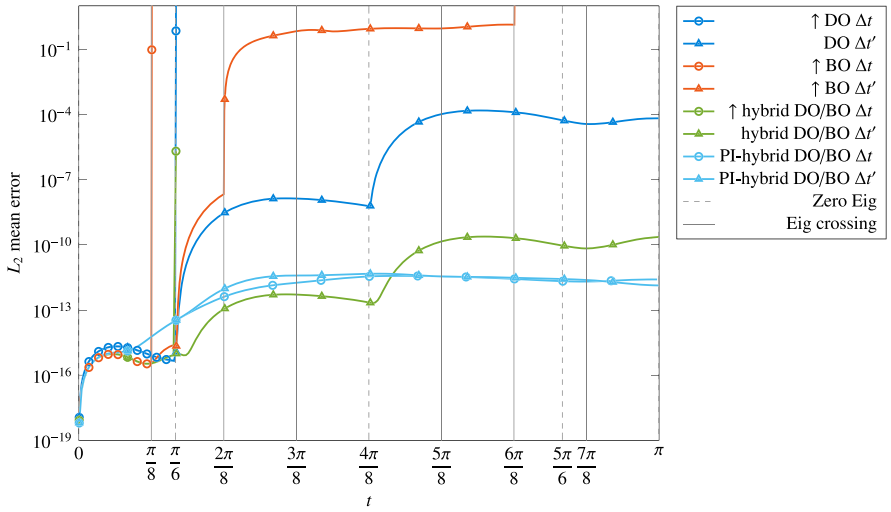

Fig. 4. Stochastic Burgers equation — effect of Δt on the performance of different methods for the Burger equation. In the above $\Delta t = \frac{\pi}{1200}$ will result in exact matching of discrete time advancement $t_{n+1} = t_n + \Delta t$ with the time of all the eigenvalue crossings and zero eigenvalues. The $\Delta t' = \frac{\pi+\epsilon}{1200}$ with $\epsilon = 0.01$ will avoid hitting the eigenvalue crossings and zero eigenvalues. In cases where the pseudo-inverse technique is used, the threshold value is $\sigma_{th} = 10^{-7}$. (For interpretation of the colors in this figure, the reader is referred to the web version of this article.)

DO/BO methods for the first few singularities, but the error still increases near singularities and the BO method eventually diverges at the eigenvalue crossing at $t = 6\pi/8$. The PI DO/BO method, on the other hand, shows stable results for both Δt values with small errors. This demonstrates the robustness gained from the pseudo-inverse technique. This robustness is useful in practical problems, where clearly the exact times of the singularities are not known *a priori*.

4.2. Kovasznay flow

We consider the Kovasznay flow whose deterministic solution is a steady, laminar incompressible flow behind a two-dimensional grid

$$\frac{\partial V}{\partial t} + (V \cdot \nabla)V = -\nabla p + \nu \triangle V + F \tag{18a}$$

$$\nabla \cdot V = 0, \tag{18b}$$

where $V = (u, v)$ is the velocity vector field, p is the pressure, ν is the kinematic viscosity and F is the forcing term. The spatial domain is $(x, y) \in [-0.5, 1.5] \times [-0.5, 1.5]$. Periodic boundary conditions in both x and y directions are enforced for mean and DO/BO modes.

Table 4
Exact BO and DO components for the stochastic Kovasznay problem with two modes, i.e. $m = 1, 2$.

	DO	BO
Mean	$\begin{pmatrix}\overline{u}(x,t)\\ \overline{v}(x,t)\end{pmatrix} = \begin{pmatrix}1-e^{\lambda x}\cos(2\pi y)\\ \frac{\lambda}{2\pi}e^{\lambda x}\sin(2\pi y)\end{pmatrix}$	$\begin{pmatrix}\overline{u}(x,t)\\ \overline{v}(x,t)\end{pmatrix} = \begin{pmatrix}1-e^{\lambda x}\cos(2\pi y)\\ \frac{\lambda}{2\pi}e^{\lambda x}\sin(2\pi y)\end{pmatrix}$
Spatial basis	$\begin{pmatrix}u_m(x,t)\\ v_m(x,t)\end{pmatrix} = \frac{1}{\sqrt{2}}\begin{pmatrix}\cos(m\pi y)\sin(m\pi x)\\ -\sin(m\pi y)\cos(m\pi x)\end{pmatrix}$	$\begin{pmatrix}u_m(x,t)\\ v_m(x,t)\end{pmatrix} = a_m(t)\begin{pmatrix}\cos(m\pi y)\sin(m\pi x)\\ -\sin(m\pi y)\cos(m\pi x)\end{pmatrix}$
Stochastic basis	$Y_1(t;\omega) = 2a_1(t)\sin(\pi\xi_1 - t)$ $Y_2(t;\omega) = 2a_2(t)\cos(\pi\xi_2 - t)$	$Y_1(t;\omega) = \sqrt{2}\sin(\pi\xi_1 - t)$ $Y_2(t;\omega) = \sqrt{2}\cos(\pi\xi_2 - t)$

For time advancement of the DO/BO modes we use an analogous splitting scheme that is used for our deterministic solver. More specifically, we use the splitting scheme that was introduced in [47]. In this fashion, in the first step of the DO/BO splitting scheme, the orthogonal projection of the explicitly evaluated nonlinear terms are added. In the second step, the pressure-Poisson is solved to project the DO/BO modes onto divergence-free space. In the last step, the viscous terms are added.

We add time-dependent random modes to the steady deterministic solution such that the solution has the form of

$$u = 1 - e^{\lambda x}\cos(2\pi y) + \sum_{m=1}^{N} u_m(x,t)Y_m(t;\omega) \tag{19}$$

$$v = \frac{\lambda}{2\pi}e^{\lambda x}\sin(2\pi y) - \sum_{m=1}^{N} v_m(x,t)Y_m(t;\omega). \tag{20}$$

In the above equations, the Reynolds number is set to be $Re = 1/\nu = 40$, and $\lambda = \frac{1}{2\nu} - \left(\frac{1}{4\nu^2} + 4\pi^2\right)^{1/2}$. We consider $N = 2$ and the spatial basis and stochastic basis are as follows:

$$(u_1(x,y,t), u_2(x,y,t)) = \frac{1}{\sqrt{2}}(\cos(\pi y)\sin(\pi x), \cos(2\pi y)\sin(2\pi x))$$
$$(v_1(x,y,t), v_2(x,y,t)) = \frac{1}{\sqrt{2}}(-\sin(\pi y)\cos(\pi x), -\sin(2\pi y)\cos(2\pi x))$$
$$(Y_1(t;\omega), Y_2(t;\omega)) = 2(a_1(t)\sin(\pi\xi_1 - t), a_2(t)\cos(\pi\xi_2 - t))$$

where $\xi_1(\omega)$ and $\xi_2(\omega)$ are independent uniform random variables on $[-1, 1]$. Then, the modes $V_i = (u_i, v_i), i = 1, 2$ satisfy the divergence-free and orthogonality conditions. The forcing term $F(x, y, \omega)$ is determined accordingly so that the above solution satisfies the Navier–Stokes equations (18). We can compute the exact components for BO and DO as shown in Table 4.

The eigenvalues of the solution are determined by $a_i(t)$ as follows:

$$\lambda_1(t) = 2a_1^2(t), \quad \lambda_2(t) = 2a_2^2(t). \tag{21}$$

We choose $a_1(t)$ and $a_2(t)$ such that they have eigenvalue crossing as well as a persistent zero eigenvalue. Specifically, we consider the following functions:

$$a_1(t) = \alpha_1, \quad a_2(t) = \alpha_2\exp(-100t^2) \tag{22}$$

where $\alpha_1 = \sqrt{1.6\times10^{-2}}$ and $\alpha_2 = 0.2$. Fig. 5(a) shows the eigenvalues in time. The eigenvalues crossing, shown by a cross symbol, occurs at $t = 0.068$, and for large times $\lambda_2(t)$ vanishes — rendering the covariance matrix singular.

For space discretization 16 elements in a quadrilateral mesh are used in the prescribed domain $(x, y) \in [-0.5, 1.5] \times [-0.5, 1.5]$. The polynomial order for the spectral element method in physical space is set to 10 and third-order Adams–Bashforth time integration is used. We use MEPCM to solve the stochastic ODE for Y_i coefficients with $Ne = 32$ elements in each random direction and $q = 4$ quadrature points in each element, resulting in 4096 collocation points in total.

We use the PI DO/BO method to solve the stochastic Kovaszany flow with $N = 2$ modes. The pseudo-inverse threshold is set to be $\sigma_{th} = 10^{-6}$, and the eigenvalue crossing threshold is set to be $\epsilon_c = 10^{-3}$. Near the eigenvalue crossing, i.e. $|\lambda_1 - \lambda_2| < \epsilon_c$, the PI DO/BO method switches from BO to DO and when the distance between the eigenvalues exceeds ϵ_c, PI DO/BO switches from DO back to BO. When the value of $\lambda_2(t)$ falls below σ_{th}, the pseudo-inverse technique is used to invert the covariance matrix. As it can be seen in Fig. 5(a), when the pseudo-inverse technique is activated, the value of $\lambda_2(t)$ is forbidden to fall below the threshold value. In the remaining of the evolution of the stochastic system, the value of $\lambda_2(t)$ stays above the threshold value, hence, the covariance matrix is inverted without using the pseudo-inverse technique. In Fig. 5(b) the L_2 error of the mean versus time is shown. It is clear that when the pseudo-inverse technique is employed, the error increases, but the error eventually stabilizes and it does not grow in time.

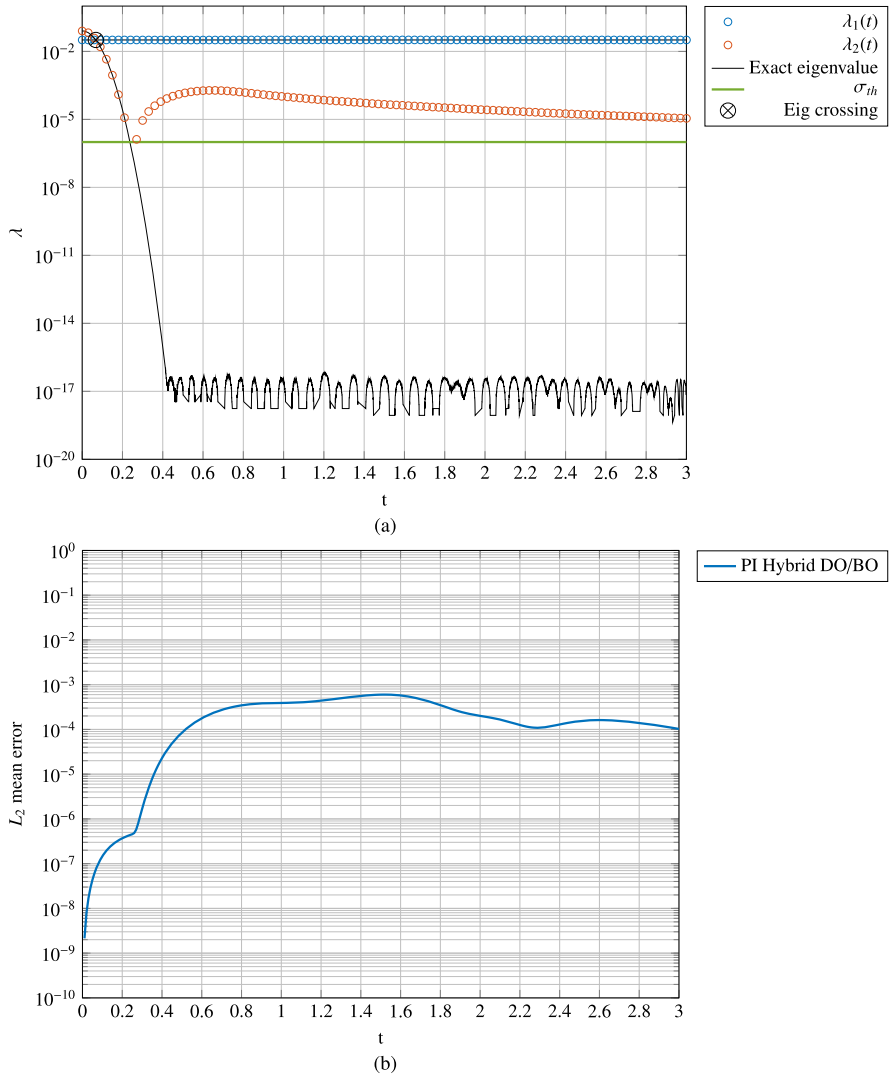

Fig. 5. Stochastic Kovasznay flow (a) Eigenvalues of the covariance matrix for the stochastic Kovasznay flow. Exact eigenvalues are shown by black solid lines and the numerical eigenvalues are shown by circles. (b) The L_2 error of the mean.

4.3. Stochastic flow over cylinder at $Re = 150$

As the last example we apply the PI DO/BO methodology to solve stochastic flow over cylinder at $Re = 150$. In particular, we focus on the adaptivity of the method by adding and removing modes to resolve the flow up to a specified threshold value. The schematic of the problem is shown in Fig. 6. We consider the flow over cylinder under stochastic forcing:

$$\begin{aligned} \frac{\partial V}{\partial t} + (V \cdot \nabla)V &= -\nabla p + \frac{1}{Re}\nabla^2 V + f_s \\ \nabla \cdot V &= 0, \end{aligned} \tag{23}$$

where the stochastic forcing is prescribed by:

$$f_s(x;\omega) = \sum_{i=1}^{N} \sigma_i a_i(t)\xi_i(\omega)\Phi_i(x),$$

where $\Phi_i(x)$ are the POD modes obtained from a deterministic DNS of the flow over cylinder at $Re = 150$. The modes are ranked such that $E_1 > E_2 > \cdots > E_N$, where E_i are the energy associated with each POD mode, and ξ_i are i.i.d. uniform random numbers $\xi_i \in \mathcal{U}[-1, 1], \quad i = 1, \ldots, N$ with unit variance.

We consider two cases of steady and time-dependent stochastic forcing with $N = 2$. We use the MEPCM to solve the stochastic ODE for Y_i coefficients with $Ne = 64$ elements in each random direction. We use one collocation point within

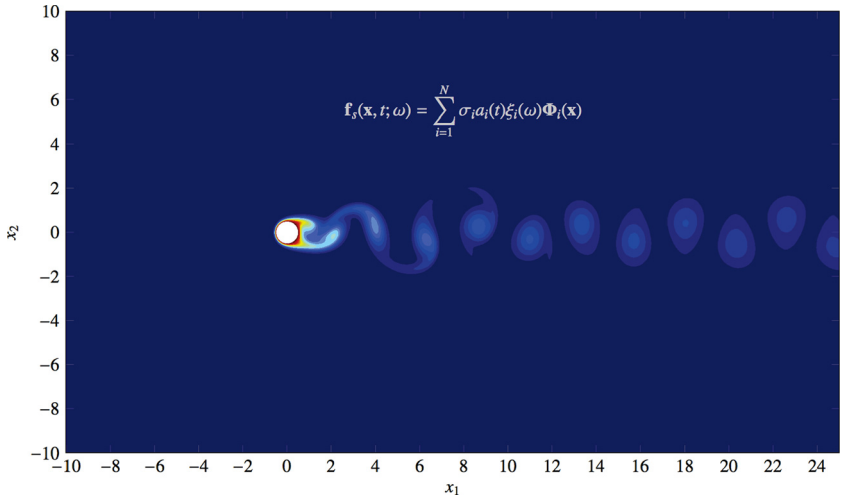

Fig. 6. Schematic of flow over cylinder at Re = 150 with stochastic forcing.

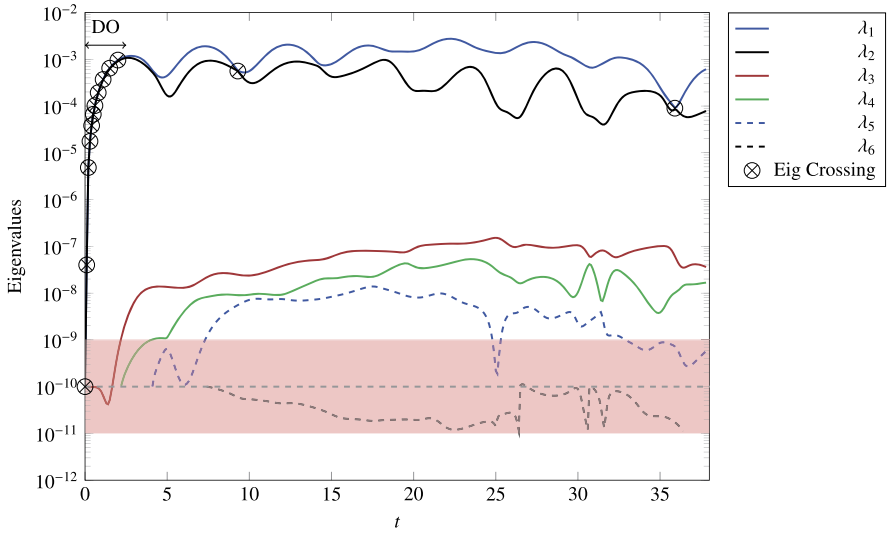

Fig. 7. The evolution of the eigenvalues of the covariance operator $E[Y_i Y_j]$ for the steady stochastic forcing for flow over cylinder at $Re = 150$. The shaded region shows the buffer zone around the energy threshold $\sigma_{th} = 1 \times 10^{-10}$. The eigenvalue crossings are marked by cross symbols. (For interpretation of the colors in this figure, the reader is referred to the web version of this article.)

each element (piece-wise constant). Therefore, in total we have $Nc = 64^2 = 4096$ collocation points. For space discretization, we use the spectral/hp element method with 4946 quadrilateral elements and polynomial order four within each element. For time discretization we use the third-order Adams–Bashforth method.

4.4. Steady stochastic forcing

First we choose a steady stochastic forcing with $a_1(t) = a_2(t) = 1$, and the standard deviation of $\sigma_1 = \sigma_2 = 0.02$. We start our simulation with $N = 2$ BO/DO modes and we then add/remove modes adaptively. The energy threshold for mode addition/removal is set to be $\sigma_{th} = 1 \times 10^{-10}$. In this example, we consider the soft-threshold criterion that, as explained in Section 3.2, in the log scale spans symmetrically around the $\log \sigma_{th}$ threshold with one decade energy depth, i.e. $d = 1$. Hence, if the energy of the last mode exceeds $\sigma_{th}^{+} = 1 \times 10^{-9}$, a new mode is added, and if the energy of the last mode falls below $\sigma_{th}^{-} = 1 \times 10^{-11}$, that mode is removed. This strategy prevents repetitive mode addition/removal as we explain below. The evolution of the eigenvalues of the covariance operator is shown in Fig. 7. At $t = 0$, we initialize two DO modes with the first two POD modes with small initial energy of $E[Y_1^2] = E[Y_2^2] = 1 \times 10^{-10}$. Note that the POD modes satisfy the orthonormality condition required for the DO modes. Since the two modes are initiated with the same amount of energy, i.e. the same eigenvalues, the active method in PI DO/BO is DO. The energy of the first two modes increases quickly and it leaves the buffer zone. This prompts the addition of the third mode in the initial stage of the evolution. As time evolves

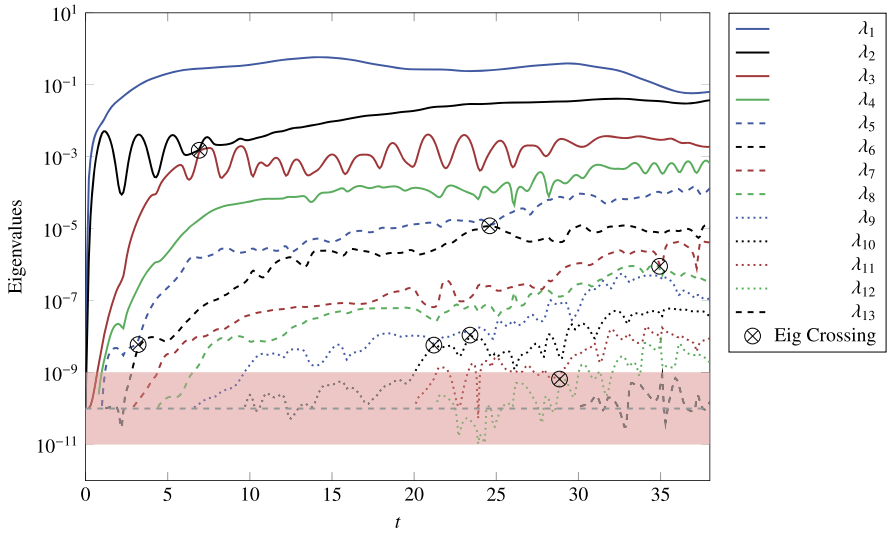

Fig. 8. The evolution of the eigenvalues of the covariance operator $E[Y_i Y_j]$ for the time-dependent stochastic forcing for flow over cylinder at $Re = 150$. The shaded region shows the buffer zone around the energy threshold $\sigma_{th} = 1 \times 10^{-10}$. The eigenvalue crossings are marked by cross symbols. (For interpretation of the colors in this figure, the reader is referred to the web version of this article.)

three more modes, *i.e.* λ_4, λ_5 and λ_6, are added. The energy of the last added mode λ_6 remains below the σ_{th} threshold, until it is eventually removed. Before the final departure at $t \simeq 36.4$, the value of λ_6 falls below σ_{th}^- at two earlier instants. However, since $\lambda_5 > \sigma_{th}^+$, λ_6 is immediately added with the energy of $\lambda_6 = \sigma_{th}$. If we do not use the buffer-zone strategy, λ_6 would cross the σ_{th} threshold repetitively, resulting in significant memory allocation/de-allocation overhead.

The energy of the first two modes remains very close for $0 < t < 2$, during which time DO is used to evolve the stochastic system. As the evolution of the stochastic flow is followed, the energy of the first two modes crosses at two other instants as marked by cross symbol in Fig. 7. In the vicinity of all these instants, the evolution of the modes is switched from BO to DO. We use the threshold value of $\epsilon_c = 10^{-3}$ for the eigenvalue crossing. Overall, the first two modes capture more than 99.99% of the total variance of the stochastic system, and the energy of all other modes combined remains negligible. This demonstrates how the PI DO/BO methodology effectively captures the two "active" modes present in the flow. As we show in the next example, increasing the variance of the stochastic forcing demands a larger number of DO/BO modes to resolve the system within the same energy threshold.

4.5. Time-dependent stochastic forcing

In this section, we use a time-dependent stochastic forcing with $a_1(t) = \sqrt{2}\sin(\pi t/2)$ and $a_2(t) = \sqrt{2}\cos(\pi t/2)$, and $\sigma_1 = \sigma_2 = 0.1$. Hence, the energy of the stochastic forcing is fives times larger than that of used with the steady forcing in the previous subsection. Similar to the steady force, we start the simulation with $N = 2$ BO/DO modes and adaptively add/remove modes as the stochastic solution evolves. We use the same threshold for the eigenvalue crossing and the same energy threshold and bounds for the buffer zone that are chosen for the steady forcing described in the previous section. The time history of the eigenvalues of the covariance operator is shown in Fig. 8. Initially, the eigenvalues of the first two modes are within the threshold of the eigenvalue crossing, i.e. $|\lambda_1(t) - \lambda_2(t)| < \epsilon_c$, and therefore, the active method in PI DO/BO is DO. The larger energy of the stochastic forcing has two clear effects on the stochastic Navier–Stokes equations. First, significant nonlinear energy transfer between the modes is observed. The nonlinear energy transfer is manifested by the large number of eigenvalue crossings – demanding a large number of switches between BO and DO methods. Note that this behavior was not observed for the small stochastic forcing described in Fig. 7. The most energetic mode considered in the large stochastic forcing considered in Fig. 8, i.e. $\lambda_1(t)$, has two order of magnitudes higher values compared to its counterpart in Fig. 7. Second, a larger number of modes are active to resolve the stochastic system up to σ_{th} threshold compared to the case with small steady forcing. As it can be seen in Fig. 8, up to time $t = 35$, twelve modes are active, and the thirteenth mode is in the buffer region. This demonstrates that for stochastic Navier–Stokes equations the number of modes to resolve the system up to a threshold value may not be known *a priori*, and an adaptive strategy is required to add/remove modes *on the fly* according to the system dynamics. As we demonstrated here, the PI DO/BO formulation can readily accommodate such an adaptive strategy.

5. Summary

In this paper, we presented an adaptive numerical method to solve stochastic Navier–Stokes equations that combines the favorable properties of the DO and BO decompositions. The hybrid method benefits from the built-in bi-orthogonality of BO

which results in diagonal mass matrices for both the system of stochastic coefficients and the spatial basis. The method only switches to DO when facing eigenvalue crossing by using an exact transformation obtained by solving a matrix differential equation. The hybrid DO/BO method is augmented with a pseudo-inverse technique to invert an ill-conditioned or a singular covariance matrix. This technique enables adaptive DO/BO representation where modes with small energy (eigenvalue) are added or removed to resolve the stochastic system up to a desired resolution. In Appendix A we show in the case of zero covariance matrix, i.e. all eigenvalues being zero, — for example a system with deterministic initial condition at $t = 0$ — the evolution of the DO spatial modes becomes equivalent to the evolution of the Optimally Time Dependent (OTD) modes, introduced in reference [4].

The DO/BO representation captures the low-dimensional structure of the SDPE, and by evolving according to the system dynamics, the DO/BO modes instantaneously follow the active subspace of the dynamical system. We have demonstrated the capabilities of the method with several examples from stochastic Burgers equation to stochastic flow over a cylinder. The robustness, demonstrated in these examples, is essential for solving stochastic Navier–Stokes equations, where nonlinear energy exchange between the modes necessitates an adaptive mode addition/removal strategy to efficiently resolve the propagation of stochasticity on a wide range of temporal and spatial scales.

Acknowledgements

This work is supported by the Office of Naval Research N00014-14-1-0166, ESRDC — Designing and Powering the Future Fleet and the DARPA grant HR0011-14-1-0060. We gratefully acknowledge their support. TPS and HB also acknowledge support by the ARO project 66710-EG-YIP. The authors sincerely thank Referee 1 for his/her comments that led to a significant improvement of this manuscript. HB gratefully acknowledges the allocated computer time on the Stampede supercomputers, awarded by the XSEDE program, allocation number TG-ECS140006.

Appendix A

In the following we show that the evolution equation of the DO spatial basis becomes equivalent to the evolution equation of the OTD modes [4] when the stochasticity approaches zero, i.e. all of the eigenvalues of the covariance operator approach zero. First, we introduce the evolution equation for the OTD modes. The readers are referred to reference [4] for more details.

Definition 1. Consider the deterministic differential equation given by

$$\frac{du}{dt} = F(u(x,t)), \quad x \in D, \tag{A.1}$$

where $u \in \mathbb{R}^n$ and $F(u(x,t)) \in \mathbb{R}^n$, and let $L \in \mathbb{R}^{n\times n}$ denote the Jacobian of $F(u(t,x))$, i.e. $L = \nabla_u F(u,t)$, then the Optimally Time-Dependent (OTD) modes denoted by $\mathbf{U}^{OTD} \in \mathbb{R}^{n\times r}$, where r is the number of OTD modes, are obtained by solving the system of coupled partial differential equations given by

$$\frac{d\mathbf{U}^{OTD}}{dt} = L\mathbf{U}^{OTD} - \mathbf{U}^{OTD}\langle \mathbf{U}^{OTD}, L\mathbf{U}^{OTD}\rangle, \quad x \in D \tag{A.2}$$

where $\mathbf{U}^{OTD}(x,t) = \{u_1^{OTD}(x,t), u_2^{OTD}(x,t), \ldots, u_N^{OTD}(x,t)\}$, and $\langle\ ,\ \rangle$ denote the Euclidean inner product. We refer to equation (A.2) as the OTD equation.

Remark 2. The OTD modes evolved by equation (A.2) remain orthonormal for all times, *i.e.* $\langle u_i^{OTD}(x,t), u_j^{OTD}(x,t)\rangle = \delta_{ij}$, for $i, j = 1, 2, \ldots, r$.

See reference [4] for the proof.

Remark 3. The OTD modes $\mathbf{U}^{OTD}(x,t)$ converge asymptotically to the least stable subspace of the differential equation (A.1).

See reference [4] for the proof.

Theorem 2. *For a differential equation with quadratic nonlinearity and zero stochastic forcing, as the covariance matrix goes to zero,* i.e. $E[Y_i^2] \to 0$ *for* $i = 1, 2, \ldots, r$, *the DO equation for the spatial modes reduces to the OTD equation.*

Proof. For a differential equation

$$\frac{du}{dt} = F(u(x,t;\omega)), \quad x \in D \tag{A.3}$$

with quadratic nonlinearity, we define $F(u(x,t;\omega))$ to be:

$$F = L_f u + q_f(u,u), \tag{A.4}$$

where L_f and q_f are linear and quadratic operators, respectively. Therefore the DO equations for the mean is given by

$$\frac{d\bar{u}}{dt} = L_f \bar{u} + q_f(\bar{u},\bar{u}) + E[Y_i Y_j] q_f(u_i,u_j), \quad i,j = 1,2,\ldots,r, \tag{A.5}$$

and for the spatial modes is given by

$$\frac{d\mathbf{U}^{DO}}{dt} C = \mathbf{F}_{\mathbf{U}^{DO}} - \mathbf{U}^{DO}\langle \mathbf{U}^{DO}, \mathbf{F}_{\mathbf{U}^{DO}} \rangle, \tag{A.6}$$

where:

$$\mathbf{F}_{\mathbf{U}^{DO}} = L\mathbf{U}^{DO} C + E[Y_i Y_j Y_k] q_f(u_j^{DO}, u_k^{DO}) \quad i,j,k = 1,2,\ldots,r,$$

where L is the Jacobian operator given by: $L(.) = L_f(.) + q_f(\bar{u},.) + q_f(.,\bar{u})$, and $C = E[\mathbf{Y}^T\mathbf{Y}]$. Multiplying both sides of equation (A.6) by C^{-1} from right results in:

$$\frac{d\mathbf{U}^{DO}}{dt} = \mathbf{F}_{\mathbf{U}^{DO}} C^{-1} - \mathbf{U}^{DO}\langle \mathbf{U}^{DO}, \mathbf{F}_{\mathbf{U}^{DO}} C^{-1} \rangle, \tag{A.7}$$

where:

$$\mathbf{F}_{\mathbf{U}^{DO}} C^{-1} = L\mathbf{U}^{DO} + E[Y_i Y_j Y_k] q_f(u_j^{DO}, u_k^{DO}) C^{-1}.$$

In the limit of zeros stochastic energy the mean equation (A.5) approaches to the deterministic differential equation:

$$\frac{d\bar{u}}{dt} = L_f \bar{u} + q_f(\bar{u},\bar{u}), \quad \text{when } E[Y_i^2] \to 0, \quad i = 1,2,\ldots r, \tag{A.8}$$

Therefore

$$\lim_{E[Y_i^2]\to 0} \bar{u}(x,t) = u(x,t), \tag{A.9}$$

where $u(x,t)$ is the solution of the deterministic differential equation (A.1). Moreover,

$$\lim_{E[Y_i^2]\to 0} \mathbf{F}_{\mathbf{U}^{DO}} C^{-1} = L\mathbf{U}^{DO}. \tag{A.10}$$

In the above limit, the term $E[Y_i Y_j Y_k] q_f(u_j^{DO}, u_k^{DO}) C^{-1}$ vanishes, since $E[Y_i Y_j Y_k] \sim \mathcal{O}(Y^3)$ and $C \sim \mathcal{O}(Y^2)$. Therefore, the DO equation for the spatial modes becomes:

$$\frac{d\mathbf{U}^{DO}}{dt} = L\mathbf{U}^{DO} - \mathbf{U}^{DO}\langle \mathbf{U}^{DO}, L\mathbf{U}^{DO} \rangle, \quad \text{when } E[Y_i^2] \to 0, \quad i = 1,2,\ldots N. \tag{A.11}$$

The above equation is the OTD equation for the differential equation (A.3). This completes the proof. □

References

[1] T. Sapsis, P. Lermusiaux, Dynamically orthogonal field equations for continuous stochastic dynamical systems, Physica D 238 (2009) 2347–2360.
[2] M. Cheng, T. Hou, Z. Zhang, A dynamically bi-orthogonal method for time-dependent stochastic PDEs I: derivation and algorithms, J. Comput. Phys. 242 (2013) 843–868.
[3] M. Choi, T. Sapsis, G.E. Karniadakis, On the equivalence of dynamically orthogonal and dynamically bi-orthogonal methods: theory and numerical simulations, J. Comput. Phys. 270 (2014) 1–20.
[4] H. Babaee, T.P. Sapsis, A minimization principle for the description of modes associated with finite-time instabilities, Proc. R. Soc. Lond. A, Math. Phys. Eng. Sci. 472 (2186) (2016), http://dx.doi.org/10.1098/rspa.2015.0779.
[5] K. Sobczyk, Stochastic Wave Propagation, Elsevier Publishing Company, 1985.
[6] V. Konotop, L. Vazquez, Nonlinear Random Waves, World Scientific, 1994.
[7] J. Fouque, J. Garnier, G. Papanicolaou, K. Solna, Wave Propagation and Time Reversal in Randomly Layered Media, Springer, 2007.
[8] T. Soong, M. Grigoriu, Random Vibration of Mechanical and Structural Systems, PTR Prentice Hall, 1993.
[9] Y. Lin, G. Cai, Probabilistic Structural Dynamics, McGraw–Hill Inc., 1995.
[10] J. Roberts, P. Spanos, Random Vibration and Statistical Linearization, Dover Publications, 2003.
[11] M. Giles, Multilevel Monte Carlo path simulation, Oper. Res. 56 (3) (2008) 607–617.
[12] A. Barth, C. Schwab, N. Zollinger, Multi-level Monte Carlo finite element method for elliptic PDEs with stochastic coefficients, Numer. Math. 119 (1) (2011) 123–161.
[13] F.Y. Kuo, C. Schwab, I.H. Sloan, Quasi-Monte Carlo finite element methods for a class of elliptic partial differential equations with random coefficients, SIAM J. Numer. Anal. 50 (6) (2012) 3351–3374.

[14] R. Ghanem, P. Spanos, Stochastic Finite Elements: A Spectral Approach, Springer-Verlag, 1991.
[15] H.G. Matthies, A. Keese, Galerkin methods for linear and nonlinear elliptic stochastic partial differential equations, Comput. Methods Appl. Mech. Eng. 194 (12) (2005) 1295–1331.
[16] R.A. Todor, C. Schwab, Convergence rates for sparse chaos approximations of elliptic problems with stochastic coefficients, IMA J. Numer. Anal. 27 (2) (2007) 232–261.
[17] X. Wan, G.E. Karniadakis, Multi-element generalized polynomial chaos for arbitrary probability measures, SIAM J. Sci. Comput. 28 (3) (2006) 901–928.
[18] H. Babaee, X. Wan, S. Acharya, Effect of uncertainty in blowing ratio on film cooling effectiveness, J. Heat Transf. 136 (3) (2013) 031701, http://dx.doi.org/10.1115/1.4025562.
[19] H. Babaee, Uncertainty Quantification of Film Cooling Effectiveness in Gas Turbines, Master's thesis, Louisiana State University, 2013.
[20] D. Xiu, J. Hesthaven, High order collocation methods for differential equations with random inputs, SIAM J. Sci. Comput. 27 (3) (2005) 1118–1139.
[21] D. Xiu, G.E. Karniadakis, The Wiener–Askey polynomial chaos for stochastic differential equations, SIAM J. Sci. Comput. 24 (2002) 619–644.
[22] J. Foo, X. Wan, G.E. Karniadakis, The multi-element probabilistic collocation method: error analysis and simulation, J. Comput. Phys. 227 (2008) 9572–9595.
[23] I. Babuska, F. Nobile, R. Tempone, A stochastic collocation method for elliptic partial differential equations with random input data, SIAM J. Numer. Anal. 45 (2007) 1005–1034.
[24] M.K. Deb, I.M. Babuška, J.T. Oden, Solution of stochastic partial differential equations using Galerkin finite element techniques, Comput. Methods Appl. Mech. Eng. 190 (48) (2001) 6359–6372.
[25] P. Frauenfelder, C. Schwab, R.A. Todor, Finite elements for elliptic problems with stochastic coefficients, Comput. Methods Appl. Mech. Eng. 194 (2) (2005) 205–228.
[26] B. Ganapathysubramanian, N. Zabaras, Sparse grid collocation schemes for stochastic natural convection problems, J. Comput. Phys. 225 (1) (2007) 652–685.
[27] X. Yang, M. Choi, G. Lin, G.E. Karniadakis, Adaptive ANOVA decomposition of stochastic incompressible and compressible flows, J. Comput. Phys. 231 (2012) 1587–1614.
[28] P. Holmes, J. Lumley, G. Berkooz, Turbulence, Coherent Structures, Dynamical Systems and Symmetry, Cambridge University Press, 1996.
[29] L. Sirovich, Turbulence and the dynamics of coherent structures, parts I, II and III, Q. Appl. Math. XLV (1987) 561–590.
[30] J. Cusumano, M. Sharkady, B. Kimble, Experimental measurements of dimensionality and spatial coherence in the dynamics of a flexible-beam impact oscillator, Philos. Trans. R. Soc. Lond. 347 (1994) 421–438.
[31] B. Feeny, R. Kappagantu, On the physical interpretation of proper orthogonal modes in vibrations, J. Sound Vib. 211 (1998) 607–616.
[32] A. Rosenfeld, A.C. Kak, Digital Picture Processing, vol. 1, Elsevier, 2014.
[33] T.P. Sapsis, Attractor local dimensionality, nonlinear energy transfers, and finite-time instabilities in unstable dynamical systems with applications to 2D fluid flows, Proc. R. Soc. A 469 (2153) (2013) 20120550.
[34] T.P. Sapsis, M.P. Ueckermann, P.F.J. Lermusiaux, Global analysis of Navier–Stokes and Boussinesq stochastic flows using dynamical orthogonality, J. Fluid Mech. 734 (2013) 83–113, http://dx.doi.org/10.1017/jfm.2013.458, http://journals.cambridge.org/article_S0022112013004588.
[35] T.P. Sapsis, H.A. Dijkstra, Interaction of additive noise and nonlinear dynamics in the double-gyre wind-driven ocean circulation, J. Phys. Oceanogr. 43 (2) (2012) 366–381, http://dx.doi.org/10.1175/JPO-D-12-047.1.
[36] E. Musharbash, F. Nobile, T. Zou, On the Dynamically Orthogonal Approximation of Time Dependent Random PDEs, Tech. Rep. MATHICSE-19-2014, École polytechnique fédérale de Lausanne, 2014.
[37] M.H. Beck, A. Jäckle, G.A. Worth, H.D. Meyer, The multiconfiguration time-dependent Hartree (mctdh) method: a highly efficient algorithm for propagating wavepackets, Phys. Rep. 324 (1) (2000) 1–105, http://dx.doi.org/10.1016/S0370-1573(99)00047-2, http://www.sciencedirect.com/science/article/pii/S0370157399000472.
[38] C. Bardos, F. Golse, A.D. Gottlieb, N.J. Mauser, Mean field dynamics of fermions and the time-dependent Hartree–Fock equation, J. Math. Pures Appl. 82 (6) (2003) 665–683, http://dx.doi.org/10.1016/S0021-7824(03)00023-0, http://www.sciencedirect.com/science/article/pii/S0021782403000230.
[39] O. Koch, C. Lubich, Dynamical low-rank approximation, SIAM J. Matrix Anal. Appl. 29 (2) (2007) 434–454, http://dx.doi.org/10.1137/050639703.
[40] T.P. Sapsis, P.F.J. Lermusiaux, Dynamical criteria for the evolution of the stochastic dimensionality in flows with uncertainty, Physica D 241 (2012) 60.
[41] M. Ueckermann, P. Lermusiaux, T. Sapsis, Numerical schemes for dynamically orthogonal equations of stochastic fluid and ocean flows, J. Comput. Phys. 233 (2013) 272–294, http://dx.doi.org/10.1016/j.jcp.2012.08.041, http://www.sciencedirect.com/science/article/pii/S0021999112005098.
[42] C. Lubich, I.V. Oseledets, A projector-splitting integrator for dynamical low-rank approximation, BIT Numer. Math. 54 (1) (2014) 171–188, http://dx.doi.org/10.1007/s10543-013-0454-0.
[43] M. Choi, T. Sapsis, G.E. Karniadakis, A convergence study for SPDEs using combined polynomial chaos and dynamically-orthogonal condition, J. Comput. Phys. 245 (2013) 281–301.
[44] Y. Rozanov, Random Fields and Stochastic Partial Differential Equations, Kluwer Academic Press, 1996.
[45] M. Loeve, Probabilistic Theory II, Springer-Verlag, 1978.
[46] T.P. Sapsis, P.F. Lermusiaux, Dynamical criteria for the evolution of the stochastic dimensionality in flows with uncertainty, Phys. D, Nonlinear Phenom. 241 (1) (2012) 60–76.
[47] G.E. Karniadakis, M. Israeli, S.A. Orszag, High-order splitting methods for the incompressible Navier–Stokes equations, J. Comput. Phys. 97 (2) (1991) 414–443, http://dx.doi.org/10.1016/0021-9991(91)90007-8, http://www.sciencedirect.com/science/article/pii/0021999191900078.